Article:
Shbeh, M.M. and Goodall, R. (2015) Design of water debinding and dissolution stages of metal injection moulded porous Ti foam production. Materials & Design, 87. 295 - 302. ISSN: 0261-3069

https://doi.org/10.1016/j.matdes.2015.08.018

Design of Water Debinding and Dissolution Stages of Metal Injection Moulded Porous Ti Foam Production

Mohammed Menhal Shbeh[1,2], **Russell Goodall**[1]

[1]Department of Materials Science and Engineering, University of Sheffield, Sir Robert Hadfield Building, Mappin Street, Sheffield S1 3JD, UK.

[2]Department of Production Engineering and Metallurgy, University of Technology, Al-Sinaa' Street, 10066, Baghdad, Iraq

Corresponding author: Mohammed Menhal, mmmshbeh1@sheffield.ac.uk

Mobile phone: +447574040497

1. Introduction

Ti foams have gained a wide interest in a variety of applications in the last decade due to them offering a unique combination of properties, such as high strength to weight ratio, high permeability and excellent biocompatibility [1]. There are several techniques for the production of Ti foams with different pore sizes and shapes, many of which are based on powder metallurgy (e.g.[2]). One such method is Metal Injection Moulding (MIM) in combination with the space holder method. MIM itself offers several advantages as a production process, and there is ongoing development of new binder systems adapted to different materials [3-5]. For foams, this technique offers several advantages over other foaming techniques, such as the potential for high volume production and the ability to produce complex near net shapes without the need for subsequent grinding and machining, which can result in closure and contamination of the pores with wear debris [6]. The MIM-space holder technique involves mixing of the metal and space holder powders with a multi-component binder and moulding them into the desired shapes before debinding and sintering. One crucial step in the success of the process is choosing the right binder and debinding it in an effective and economical way. There are two main methods for debinding, namely thermal debinding and solvent debinding. The former usually results in more contamination and needs to be done carefully and at a slow rate to avoid the formation of cracks and slumping of the samples [7]. The latter is usually carried out in either water or other solvents such as hexane. Hitherto, most of the reports on the production of Ti foams via MIM-space holder method used paraffin wax as a major binder constituent and organic solvent debinding for binder removal [8, 9]. However, one significant problem is that the debinding and

space holder removal processes can often take a very long time (up to 72 hours) [10]. Another problem is that environmentally unfriendly organic solvents are used for paraffin wax debinding such as Chloroform [9] and hexane [8, 10, 11]. In this paper, the use of water soluble polymer, namely Poly ethylene glycol (PEG) as a main constituent in the binder and its debinding behaviour will be studied for the production of Ti foams by the MIM-space holder method. In addition, different water debinding and space holder dissolution techniques will be explored and a comparison will be made among those techniques. Furthermore, the effect of the temperature on the removal of the binder and space holder will be examined. This knowledge will allow the design of a more efficient process.

2. Experimental Procedure

2.1. Starting Materials

Commercially pure Ti grade 2 (Arcam AB, Sweden) powder with spherical particles was used in this study. The particle size distribution of the Ti powder was analysed via a Malvern Mastersizer 3000 using the wet dispersion method. Potassium chloride (Sigma-Aldrich, Steinheim, Germany) was used as a space holder and its particle size distribution was analysed using a Malvern Mastersizer 3000 with the dry analysis method. Table 1 summarises the size distribution and density of the powders used. The morphologies of both the Ti powder and KCl space holder are shown in figures 1a and 1b. The space holder was sieved through a 500 micron sieve. The binder consisted of PEG1500 (Sigma-Aldrich, Steinheim, Germany), Poly methyl methacrylate (PMMA, Sigma-Aldrich) and stearic acid with purity of ≥97% (Fluka, Sigma-Aldrich). The density of the powders and binder constituents were measured using an AccuPyc II 1340 Pycnometer, Micromeritics, USA.

Table 1. Characteristics of Starting Materials

Name	Dx (10)	Dx (50)	Dx (90)	Density, g/cm^3
Ti Powder	52 µm	72.5 µm	102 µm	4.5371
KCl Powder	188 µm	307 µm	476 µm	1.9866
PEG 1500	-	-	-	1.1300
PMMA	-	-	-	1.2060
Stearic Acid	-	-	-	1.0075

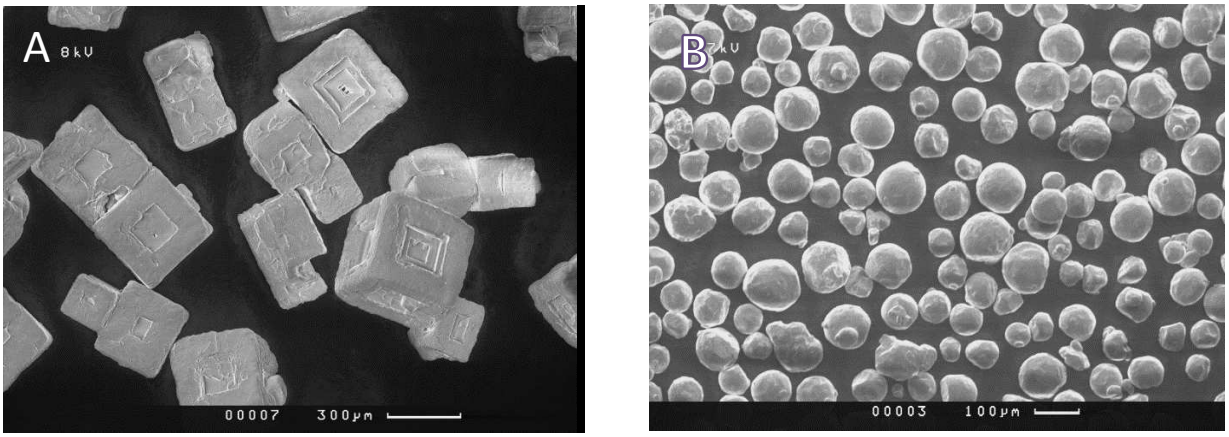

Figure 1. A. KCl Powder, B. Ti powder

KCl particles were cubic with a hopper-like shape in some cases. This shape usually results from a crystal growth mechanism where atoms add preferentially at the edges, leading to a faster growth at the edges compared to the centre. Ti particles, produced by gas atomisation, were approximately spherical in shape.

2.2. Feedstock preparation

The feedstock was prepared by mixing the Ti powder with the KCl space holder using a centrifugal Speedmixer 800 FZ (Hauschild; supplied by Synergy Devices Ltd, UK). Four cylindrically shaped dispersion media made of zirconia were added to mixture. Next, PMMA and stearic acid were added to the mixture and the mixing process continued according to the following mixing program.

Table 2. Mixing Programme of Feedstock

Mixing Speed (rpm)	1300	1600	1800	1400	1600	1800
Time, (minutes)	4	4	2	2	2	2

The mixing programme was chosen so that the heat generated from friction as the constituents mix was sufficient to melt the PMMA. It consists of 2 sets of increasing speeds, intended to build up the heat each time. PEG was added in the last three stages of the mixing programme in order to guarantee that the PMMA first gets melted and homogenised in the mixture before adding the PEG, as the latter has a low melting temperature in comparison with the former. It should be noted that the temperature of the mix cannot be directly measured in the equipment, so visual observation of molten state was used to determine when the temperature was sufficient. The total period of mixing, 16 minutes, is much shorter than that reported in the literature (e.g. over 1h for the same binder components for MIM of stainless steel powder, with a blade mixer at

a speed of 30rpm and a temperature of 70℃ [12].) due to the effectiveness of the high speed centrifugal mixer with the dispersion media in mixing and homogenising the powders and polymers. The mixture was then pelleted by extruding it twice through a plunger type injection molder at 150 ℃ and cutting it into small pellets. The pellets were then allowed to cool for five minutes before carrying out any subsequent processing. The volume percentage of the solid part was equal to 55 % of which 50 % was space holder and 50 % was Ti, while the volume percentage of the binder was equal to 45 % of which 65 % PEG, 30 % PMMA and 5 % stearic acid.

2.3. Differential Scanning Calorimetry (DSC) and Thermogravimetric (TG) Analyses of the Binder

These analyses were performed in order to find out the melting and decomposition behaviour of the binder and according to which the injection temperature and debinding temperature were set. The DSC analysis of the binder and its constituents was performed using a DSC 6, Perkin Elmer, USA. The thermogravimetric analysis was carried out under argon atmosphere using a Pyris 1 TGA instrument, Perkin Elmer, USA.

2.4. Rheological Characteristics of the Feedstock

The viscosity of the feedstock was measured using a twin bore barrel capillary rheometer (Rosand RH2000, Malvern, UK). The test was carried out at 150 °C and at a shear rate in range of 900 to 5000 s^{-1} using a tungsten carbide die. The die had a diameter of approximately 2 mm and a length of 16 mm. Rabinowitsch correction was applied to the results in order to get absolute viscosity readings by correcting the shear rate value and obtaining the true shear rate as

the flow of the feedstock is pseudoplastic (non-Newtonian) [13]. The flow behaviour index was calculated using the following power law equation [14]:

$$\eta = K\dot{\gamma}^{n-1} \quad (1)$$

where η is the viscosity, K is a constant, $\dot{\gamma}$ is the shear rate and n is the flow behaviour index, which is equal to 1 for Newtonian fluids and less than 1 for pseudoplastic fluids.

2.5. Sample Preparation

Small cylindrical parts were injection moulded at a temperature of 150 °C and pressure of 45 MPa using a plunger type injection moulder (J.B. Engineering, United of Kingdom). The specimens were 10 mm in diameter and 6 mm in height. One green sample was broken and its surface was gold coated by sputtering for 3 minutes in order to investigate the surface of the sample using Scanning Electron Microscopy (Camscan Mk II, Cambridge Scanning, UK).

2.6. Solvent Debinding and Dissolution of the Space Holder

One advantage of using partially water soluble binder is that fraction of the binder and the space holder can be removed in one process unlike other binders where organic solvent debinding and water dissolution are required and have to be carried out separately. The water soluble part of the binder and space holder were removed by water dissolution using different techniques. The first technique was performed by real time monitoring of weight loss of both the binder and space holder using a Mettler Toledo density balance with resolution of 0.1 mg. The sample was put on the weighing basket of the density balance under water and weight loss was recorded with time. The temperature was recorded using a thermometer supplied with the density balance. The

following equations were used to calculate the percentage of space holder and binder removed with time:

$$P_{KCl+PEG} = \frac{W_i - W_t}{W_i - W_f} \times 100\ \% \quad (2)$$

$$W_f = (w_{Ti} + w_{PMMA} + w_{SA}) \times W_i \quad (3)$$

where:

$P_{KCl+PEG}$: The percentage of binder and space holder removed

W_i: The initial weight of the sample (in water in the case of the first experiment and in air in the case of other experiments)

W_t: The weight of the sample at time t

W_f: The expected weight of the sample after complete dissolution of the water soluble space holder and binder components

w_{Ti}: The weight fraction of Ti

w_{PMMA}: Weight fraction of PMMA

w_{SA}: Weight fraction of stearic acid

Although stearic acid can be dissolved in water to a certain extent and its solubility increases as the water temperature rises [15], it was assumed to be insoluble in the first experiment as the temperature was relatively low (20 °C). The second technique was performed using an ultra-sonic bath at room temperature. The sample was weighed in air using Mettler Toledo balance

with resolution of 0.1 mg and then put on the metal gauze of the ultrasonic bath and vibrated ultra-sonically. The weight loss was monitored with time by taking the sample out of the bath every 15 minutes and drying it using heated compressed air for 15 minutes before weighing the sample three times at different intervals in order to make sure that a consistent reading was taken. The third technique was done using heated ultrasonic bath supplied with a thermostat and built in thermometer in order to have precise control over temperature. The temperature was set to 50 °C (set according to the DSC analysis of the PEG) and the sample was ultrasonically vibrated. Every 15 minutes, the sample was taken out of the bath and dried using similar drying procedure to the second experiment followed by weight loss measurement. The fourth dissolution technique was performed using a hot plate stirrer with magnetic bar to mix the water vigorously. The sample was put on a metal basket and hung using a metal stand. The basket was placed inside a 1000 ml water beaker. The beaker was put on a hot plate stirrer. The rotation speed of the magnetic bar was set to 900 rpm while the temperature was set so that the water temperature inside the beaker was equal to 50 °C. The temperature was monitored using a digital thermometer with a K-type thermocouple (Digitron TM22, England). The drying procedure and weight loss measurement were performed in a similar manner to the previous experiments. In calculations for these experiments, equation 3 was used without inputting a value for the weight fraction of stearic acid (w_{SA}) as at 50°C stearic acid dissolves much more easily in water than at 20°C [15], and is considered therefore not to contribute to the final weight.

2.7. The Effect of Temperature on dissolution of Space Holder and Binder

Specimens were placed on a metal basket of a heated bath at different temperatures. The temperatures were decided according to the melting temperature of PEG which was obtained through DSC analysis (found to be 50.12 °C). The dissolution processes were carried out at three

different temperatures below the melting temperature of the PEG and three temperatures above the melting temperature of PEG in order to understand the effect of temperature on the dissolution of binder and space holder. The first set of temperatures were 25, 30 and 40 °C, whereas the second set of temperatures were 60, 70 and 80 °C. The debinding and dissolution processes were carried out for three hours at these sets of temperatures. The samples were taken out of the bath every hour in order to measure the weight loss. The samples were dried and weighed using similar technique to that mentioned previously. The cubic root of mass was calculated and plotted against time in order to find the dissolution rate constant (K) for each temperature using the Hixson–Crowell cube root law.

$$\sqrt[3]{m} = \sqrt[3]{m_i} - Kt \quad (4)$$

where:

m: The remaining mass of binder and space holder at time t

m_i: The initial mass of binder and space holder

K: The dissolution rate constant, also counting the temperature-dependent component of the rate

t: time in seconds

After calculating the dissolution rate constant for each temperature, an Arrhenius plot was constructed by drawing the logarithm of K against the inverse temperature. Finally, the activation energy for the dissolution process was calculated by calculating the negative slope of Arrhenius plot and multiplying it by the gas constant (8.314 J/mol.K).

2.8. Thermal Debinding and Sintering of Samples

The removal of the high viscosity part of the binder (PMMA) and sintering of samples were performed in one cycle using a tube furnace under an inert atmosphere (argon) according to the thermal profile in figure 2.

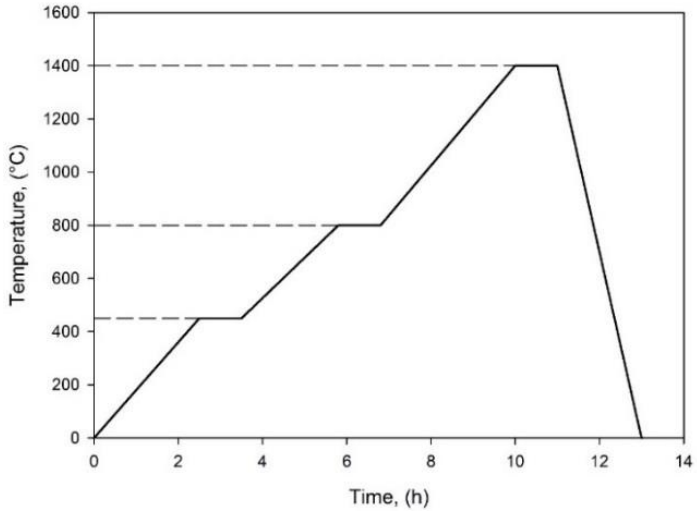

Figure 2. Thermal debinding and sintering cycle

The samples were firstly heated to 450℃ for 1 hour in order to ensure the complete removal of PMMA according to the TGA results. There was then a dwell at 800 ℃ for pre sintering to give some initial structural integrity (a common practice in powder production of foams [16, 17]) before sintering them at 1400℃ for 2h. The true densities of the material making up the foams (only the solid part) were measured using a pycnometer (AccuPyc II 1340, Micromeritics, USA), whereas the bulk densities of the foams were measured using Archimedes' principle after sealing the surface of the samples with a layer of high vacuum grease.

3. Results and Discussion

3.1. DSC and TGA Results

The results of the DSC analyses of the binder and its constituents are shown in figure 3. As can be seen from figure 3 that the peak melting point of PEG was shifted to the left in the presence of PMMA (i.e. lowered from 50.12 °C for pure PEG 1500 to 48 °C for PEG in binder). Whereas the peak melting temperature of the PMMA was shifted to the right (i.e. increased from 126 °C for pure PMMA to 139 °C in the presence of PEG). This is an indication of interaction among the binder polymers where the crystalline PEG interacts with the amorphous PMMA resulting in a blend of some amorphous regions with crystalline regions composed of PEG entirely. Jian and Guoqin [18] studied the behaviour of interaction between PEG and PMMA and found that PEG and PMMA can form semi-interpenetrating polymer-networks that are composed of mixtures of crystalline and amorphous regions when the PEG content is greater than 35 wt %. Thus, in order to make sure that all the binder components are melted, a temperature of 150 °C was chosen for further investigations and sample preparation. Furthermore, a temperature of 50 °C was chosen for some of the dissolution and debinding processes to guarantee PEG melting.

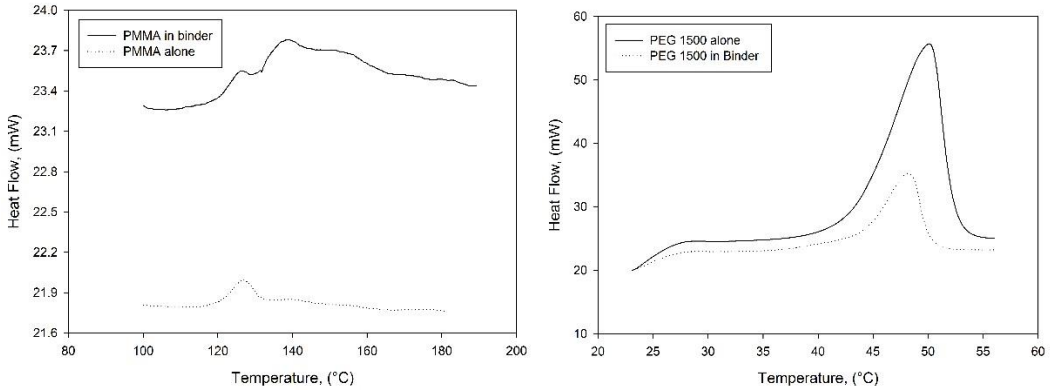

Figure 3. DSC results of PMMA and PEG.

The results of TGA analyses of the binder (PEG, PMMA and SA) and pure PMMA are shown in figure 4.

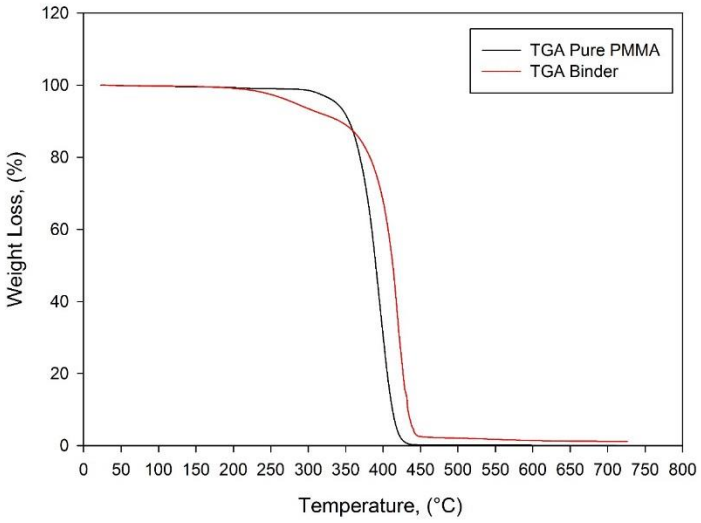

Figure 4. TGA results of the binder and pure PMMA

It can be noted from figure 4 that pure PMMA was completely decomposed at approximately 430 ℃, whereas almost all of the binder was decomposed at a temperature of 450℃. This means that the thermal debinding stage should be carried out at a temperature equal or above 450 °C in order to guarantee the removal of components remaining after water debinding and dissolution of the space holder. The binder shows a higher decomposition temperature than pure PMMA because of interaction among the binder components. Thus, it is expected that PEG removal will be harder than its debinding in the pure form. In addition to this, several factors will affect the removal of PEG from the samples, including the percentage of PMMA in the binder, the particle size and shape of the injected powder as well as the molecular weight of the PEG used [19].

3.2 Rheological Analysis Results

The result of the viscosity analysis of the feedstock is shown in figure 5.

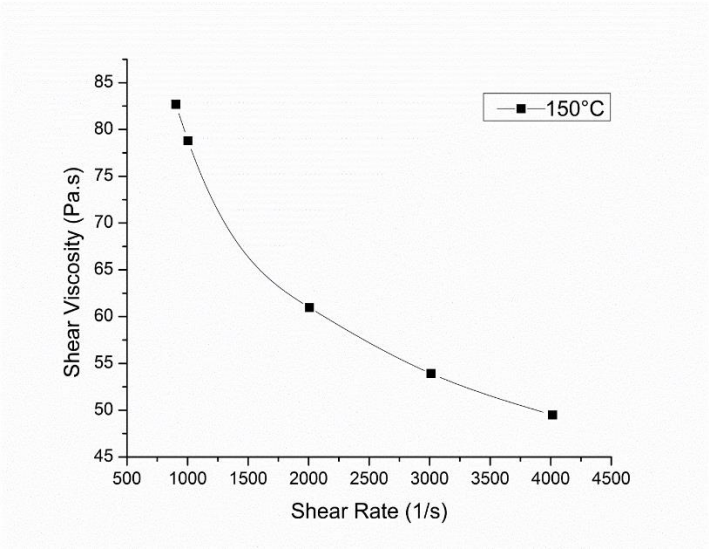

Figure 5. Viscosity Analysis of feedstock

As can be seen from Figure 5, as the shear rate increases, the viscosity of the feedstock decreases. This is an indication that the feedstock shows some shear thinning behaviour which is preferred for the MIM process, especially in producing complex shapes. The shear sensitivity value (n) was approximately equal to 0.655. It is believed that this drop in viscosity occurs due to the re-orientation of particles and breakage of agglomerates [20]. However, some argue that this phenomenon takes place due to reduced friction and unfolding of polymer chains at high shear rates [21]. It was reported that the viscosity of the MIM feedstock should be less than 1000 Pa.s in the shear rate range of 10^2-10^5 (1/s) [20]. Thus, the viscosity of the feedstock meets the criteria to be successfully injection moulded.

3.3 SEM Analysis Results

Figure 6 illustrates the morphology of the broken sample which was imaged using SEM at 6 kV.

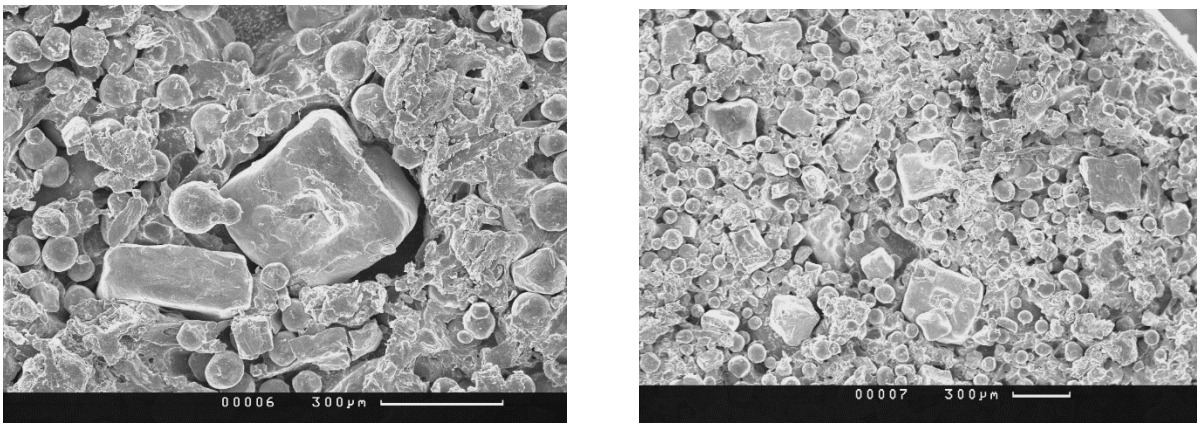

Figure 6. SEM images of the surface of as-broken green sample

It can be noted that the KCl particles remain cubic in shape and are not coated with the binder to the same extent as the Ti powder. This can be helpful for rapid removal of the space holder from the sample by water dissolution where water penetrates into the specimen faster and breaks up the ionic lattice of the KCl resulting in solvated ions.

3.4 Debinding and Dissolution Results

The results of different water debinding and dissolution techniques are shown in figure 7. It can be noted that the ultrasonic water debinding and dissolution at a temperature of 50 °C was the quickest method in comparison with other water debinding and dissolution techniques, where the PEG and space holder were completely removed after 4 hours. The hot plate stirring method came second with double the removal time of the heated ultrasonic bath method. The third and last methods were ultrasonic dissolution at ambient temperature and dissolution at 20 °C. It can also be seen from figure 7 that the linear parts of the curves of the heated ultrasonic dissolution and hot plate stirring were much larger compared to the other two methods. This is due to the fact that temperature has a great impact on the removal rate of both space holder and PEG, the latter especially as the melting temperature of PEG (50°C) were reached in the experiments.

Hence studying the temperature effect would be a matter of great importance in the removal rate of PEG and space holder. Furthermore, it can also be observed that the removal rates were approximately equal for the heated ultrasonic and hot plate stirring dissolution in the initial stages of water debinding and dissolution, but this trend changes with time in favour of the heated ultrasonic bath. This is due to the high efficiency of the ultrasonic vibrations in removing the dissolved space holder and PEG faster from the inside of the sample and consequently lifting the limitation of the rate being controlled by the diffusion process of the dissolved space holder and PEG to the outer surface. This has been considered previously as the bottleneck in slowing the removal process of the space holder and PEG from the sample [22-24].

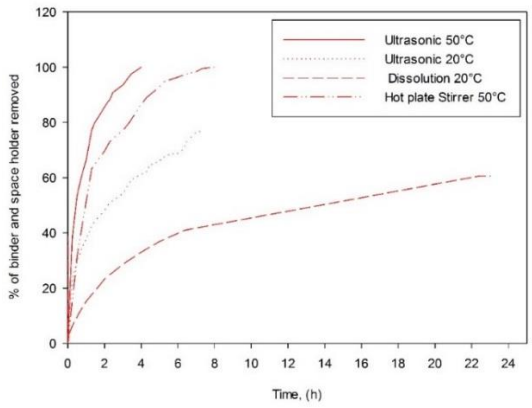

Figure 7. Results of Different Debinding and Dissolution Methods.

It can also be noticed that the real time monitoring of water debinding and dissolution using a density balance gives a smooth curve over time. However, the complete removal of space holder and PEG was not realised. This can be attributed to the low temperature of the experiment (20°C) compared to the peak melting temperature of PEG (50°C). SEM images of the 20°C water debinded specimen are shown in figure 8.

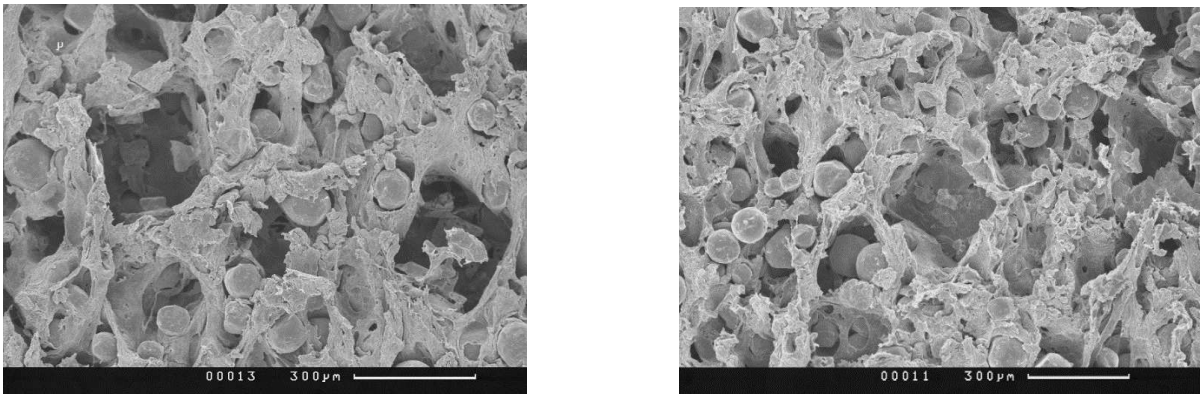

Figure 8. SEM Images of the sample after 23 hours of dissolution

As can be seen from the SEM images, the KCl space holder was dissolved in water and the shape of pores replicated the shape of the space holder, while the PEG and PMMA networks are still apparent after 23 h of dissolution at 20°C. These networks can be eliminated by increasing the temperature of the dissolution up to or above the melting temperature of PEG.

3.5 Temperature Analyses Results

Figure 9 indicates the results of debinding and dissolution at different temperatures

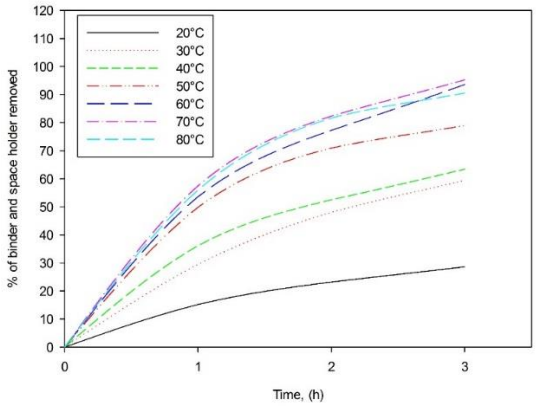

Figure 9. Dissolution curves at different temperatures

In general, as the temperature of the dissolution increases, the rate of the removal of the space holder and PEG rises. This is due to faster removal of PEG and KCl at higher temperatures, especially when the temperature reaches the peak melting point of PEG (50°C). However, this trend changes as the dissolution temperature reaches 80°C where the removal rate becomes slower than that at 70°C particularly after longer dissolution times. This is suspected to be due to the fact that under these conditions the sample was significantly swollen, making it much harder for the space holder to be removed. Observations of the samples after dissolution found that the sample's surface area at 80°C had swelled by around 20 %. This might be due to water uptake by the binder and on a microscale; such swelling could close the channels through the structure, reducing the dissolution rate. Thus, it is not recommended to carry out water dissolution at a temperature higher than 70°C. In addition, the data for the 80°C experiment were not used in constructing the Arrhenius plot, as another mechanism is thought to have been activated. The percentage of space holder and binder removed after three hours of dissolution at 70°C is equal to 95 %, whereas only 28 % was removed after 3 hours of dissolution at 20°C. An example of cube root mass plot obtained under equation 3 for the 30°C experiment is shown in figure 10 a. All the tests at different temperatures showed a similar degree of fit. The correlation values for the plotted root mass curves were ranging from 0.95 to 0.99. The Arrhenius plot obtained is illustrated in Figure 10 b.

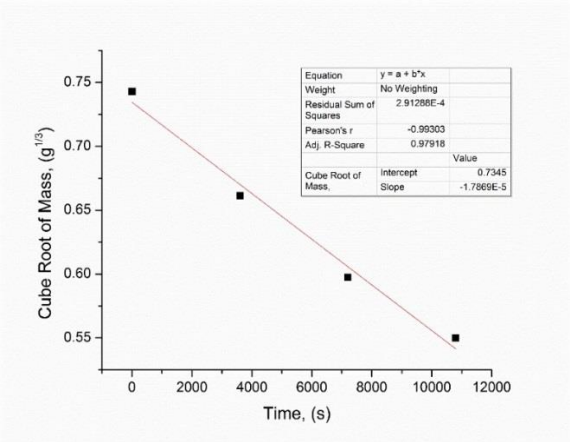

(a)

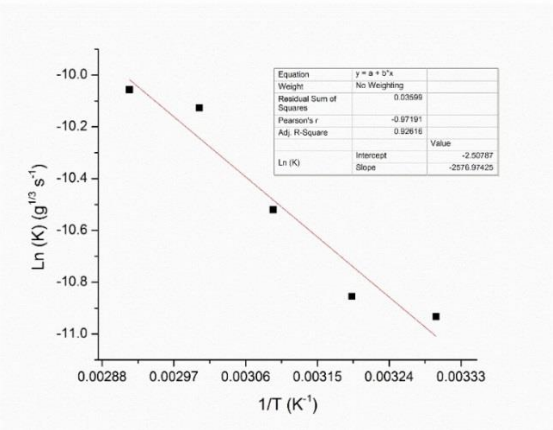

(b)

Figure 10 A. A plot of cube root mass against time for the 30°C experiment, B. Arrhenius plot for water debound MIM-SH foams at different temperatures

The fact that these plots show a straight line indicates that the Hixson–Crowell law applies in the first stages of the dissolution and that the process at this stage is not controlled by slow rate diffusion, thus diffusion does not play a significant role in the first stages of dissolution. However, its importance in determining dissolution time would be expected to increase at later stages in the dissolution process or where samples have larger size (with additional dependency on sample shape, debinding technique and percentage of space holder). It is also interesting to note that there is not a dramatic departure from the linear fit as the temperature passes the measured peak melting point of the PEG, 50 °C.

The activation energy for the dissolution process was found to be equal to 21.4 kJ/mol. This value is comparable to the value reported in the literature for dissolution of PEG from injection moulded dense Ti parts, namely 21.5 kJ/mol and approximately equivalent to the attraction energy between the water molecules (23.3 kJ/mol)[23, 25]. Thus, PEG plays an influential role in the dissolution process and is the main barrier for accelerating the dissolution process. By

contrast, the KCl does not act as the rate controlling phase. The dissolution process takes place by interaction of water molecules with PEG and KCl. KCl dissolves faster than PEG leading to the creation of macropores that replicate the shape of KCl particles. These macropores promote rapid water penetration through the sample. Depending on the dissolution temperature, the hydration process of PEG molecules begins and proceeds at a particular rate. These hydrated PEG molecules move out of the sample leaving amorphous networks of PMMA behind and creating micropores. These amorphous PMMA networks are responsible for providing mechanical stability for the parts after dissolution, but before sintering (the green state).

3.6 Sintering Results

To validate that the materials processed were suitable for the production of titanium foams, several samples were sintered. Some sintered samples are shown in figure 11a, while an SEM image of as-sintered foam surface is shown in figure 11b.

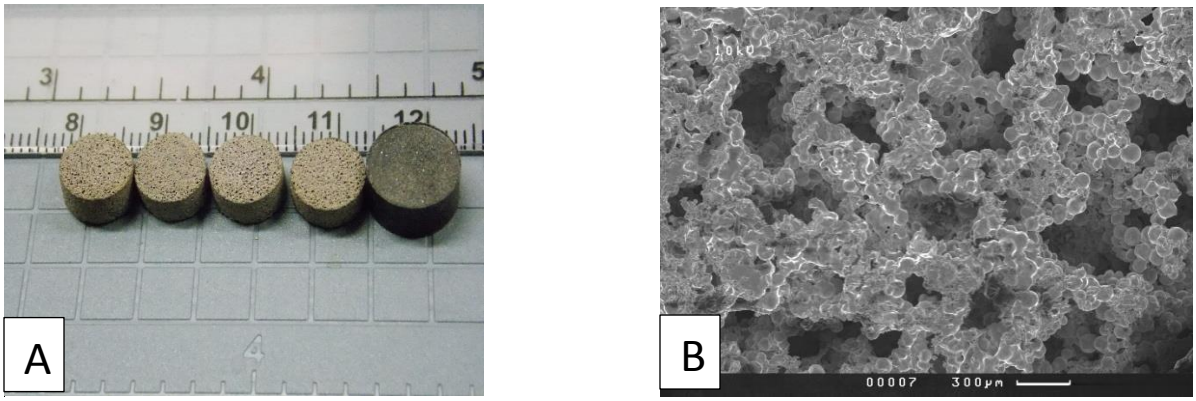

Figure 11. A. Un-sintered and sintered samples. B. As sintered sample surface

As can be seen the shape of the pores have been altered during the sintering process from a cubic shape to approximately elongated irregular pores, though the size of the pores is still proportional to the size of the space holder particles. This change in the shape of the pores is believed to be

due to shrinkage during sintering under a relatively high sintering temperature (1400℃) in comparison with what is typically used in the literature (1100-1200℃) [10, 26]. The diameter of the samples shrank by 16.5% to become around 8.6 mm after sintering, while the height of the samples shrank by 12 % to be equal to 5.3 mm. It also can be noted that the inner cell walls of the foams are microporous. These micropores will act as microporous bridges connecting the macropores, and should thus lead to higher porosity and permeability. Although some argue that these micropores can be beneficial (e.g.in transporting body fluids and nutrients in biomedical applications [27]), the presence of such micropores can negatively impact the mechanical properties of foams by reducing the load bearing cross sectional area of the cell walls [28]. The true density was found to be equal to 4.5 g/cm^3 which is equivalent to the density of Ti and an indication that all pores present are open pores, whereas the foam density was equal to 2.005 g/cm^3 meaning that the volume percentage of porosity is equal to 55%. This percentage is much higher than the volume percentage of the space holder which was about 27.5% vol. This could be attributed to the entrainment of voids from the feedstock, though where this is observed acetone is often included as a solvent, so an alternative explanation could be a significant amount of microporosity. The presence of this quantity of micropores can be attributed to several factors such as the relatively large particle size of the starting powders and the quantity (45vol%) and nature of binder system used (PMMA,PEG and SA) which is reported to lead to micropores [29]. Increasing the space holder percentage has been observed to lead to decreased cell wall thickness and reduced chances for the formation of micropores among the powder particles [30, 31].

One critical issue in producing Ti parts by MIM is carbon and oxygen contamination during processing (mainly during debinding and sintering stages). It has been shown that the binder system used can give low content of these interstitial elements [32]. Carbon, oxygen and nitrogen

content in the foams produced were assessed using a LECO melt extraction system by AMG Analytical, UK. Chlorine content was also assessed as a means to check the removal of the KCl. The results are shown in table 3, and are compared with a Ti foam produced by MIM in the literature using NaCl as a space holder and a binder composed of PEG, low density polyethylene, paraffin wax and SA [26].

Table 3. Interstitial analysis of the foams produced.

Foam	Vol% Space holder	Vol% binder	Sintering Temperature, °C	% porosity	C %	O %	N%	Cl %
Ti foam, Vacuum Furnace	36	40	1400 for 2h	56	0.091	0.786	0.026	<0.01
Ti foam, Tube Furnace	27.5	45	1400 for 2h	55	0.672	0.730	0.042	<0.01
Ti foam [26]	25	50	1200 for 4h	36	0.17	0.66	0.020	-

The results indicate that the type and cleanliness of the furnace used play a significant role in dictating the extent of contamination during debinding and sintering as the carbon content for foams produced in a vacuum furnace was much less than that for foams produced in a tube furnace under flowing argon. The level of oxygen is also quite high for titanium foams generally, which would be expected to impact the mechanical properties, a result that is comparable to material from the literature. This problem can be addressed by improving the vacuum of the sintering environment and reducing the sintering temperature [33, 34]. The low chlorine content indicates that KCl removal has been largely successful.

4. Process Design of the Debinding Stage

As noted earlier, the debinding stage makes up the dominant fraction of the time required for the processing of titanium foams by MIM in most currently reported methods. To achieve a feasible processing time industrially, this should be minimised. As expected, and shown above, increasing the temperature is one way to do this, yet this also comes with an associated cost. The balance between the two may vary with different applications, and so a selection diagram has been created, based on the data found here (Figure 12). As the moment of complete dissolution is difficult to determine precisely, this chart is constructed taking the time to 60% dissolution as a representation of the dissolution speed. It shows that, while many different sets of conditions could be optimum, depending on the relative importance of keeping temperature or time low, the ultrasonic method would always be preferred, and the optimum conditions for an equal weighting of low time and temperature would be estimated to be ultrasonic conditions at 50°C. It should be noted that as the time will vary depending on many characteristics these values are indicative of the relative differences between the processes only.

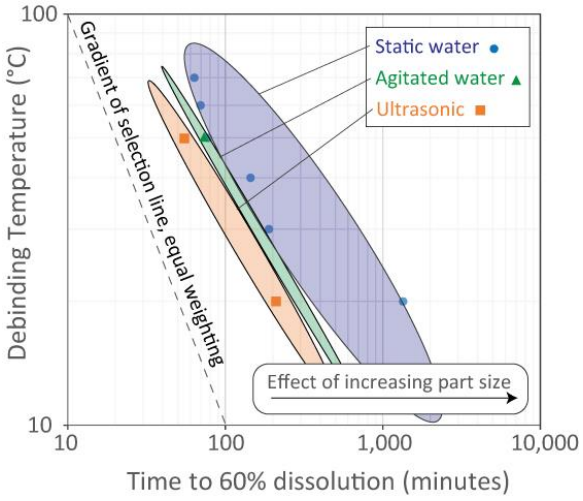

Figure 12. A selection diagram for the different debinding processes explored, showing the trade-off between dissolution temperature and time. The data points from this study are plotted, along with indicative envelopes of the ranges they occupy. A selection line following Ashby's method is included for the gradient when minimisation of each parameter is of equal importance.

Conclusion

In conclusion, the effect of variations in the water debinding step on the potential production time of Ti foams has been investigated. Cylindrical samples initially moulded at 10mm diameter and 6 mm height produced foams of around 8.6 mm diameter and 5.3 mm height after processing. Ultrasonic water dissolution at the peak melting temperature of PEG was the fastest way of water debinding and dissolution where the space holder and PEG were completely removed within four hours. Hot plate stirring was second fastest method with a total removal time of 8 hours. It was also found in this study that the dissolution temperature can play an important role in increasing the removal rate of PEG and space holder. The best temperature for dissolution was found to be equal to 70°C, above which the rate of dissolution was reduced due to a significant swelling in the sample that slows the removal process of the space holder. The activation energy for the dissolution process was found to be 21.4 kJ/mol, consistent with the dissolution of PEG. These results allow design decisions to be made depending on the required characteristics for a particular applications.

Acknowledgements

This work was financially sponsored by the Iraqi Ministry of Higher Education and Scientific Research. The authors would like to thank Mr. Ben Palmer for his support during TGA Analysis.

References

1. Goodall, R., *Porous metals: foams and sponges.* Advances in Powder Metallurgy: Properties, Processing and Applicatons, 2013(60): p. 273-307.
2. Mondal, D.P., et al., *Titanium foam with coarser cell size and wide range of porosity using different types of evaporative space holders through powder metallurgy route.* Materials & Design, 2014. **63**: p. 89-99.
3. Arifin, A., et al., *Powder injection molding of HA/Ti6Al4V composite using palm stearin as based binder for implant material.* Materials & Design, 2015. **65**: p. 1028-1034.
4. Gulsoy, H.O. and C. Karatas, *Development of poly(2-ethyl-2-oxaline) based water-soluble binder for injection molding of stainless steel powder.* Materials & Design, 2007. **28**(9): p. 2488-2491.
5. Karatas, C., et al., *Investigation of mouldability for feedstocks used powder injection moulding.* Materials & Design, 2008. **29**(9): p. 1713-1724.
6. Bram, M., et al., *Investigations on the machining of sintered titanium foams utilizing face milling and peripheral grinding.* Advanced Engineering Materials, 2003. **5**(6): p. 441-447.
7. Bakan, H.I., *Injection moulding of alumina with partially water soluble binder system and solvent debinding kinetics.* Materials Science and Technology, 2007. **23**(7): p. 787-791.
8. Deing, A., et al., *A Porous TiAl6V4 Implant Material for Medical Application.* Int J Biomater, 2014. **2014**: p. 904230.
9. Guoxin, H., et al., *Fabrication of high porous NiTi shape memory alloy by metal injection molding.* Journal of Materials Processing Technology, 2008. **206**(1-3): p. 395-399.
10. Tuncer, N., et al., *Study of metal injection molding of highly porous titanium by physical modeling and direct experiments.* Journal of Materials Processing Technology, 2014. **214**(7): p. 1352-1360.
11. Barbosa, A.P.C., et al., *Realization of a Titanium Spinal Implant with a Gradient in Porosity by 2-Component-Metal Injection Moulding.* Advanced Engineering Materials, 2013. **15**(6): p. 510-521.
12. Rajabi, J., et al., *The effect of nano-sized stainless steel powder addition on mechanical and physical properties of micropowder injection molded part.* Materials & Design, 2014. **63**: p. 223-232.
13. Schramm, G., *A practical approach to rheology and rheometry*. 1994: Haake Karlsruhe.
14. Huang, B.Y., S.Q. Liang, and X.H. Qu, *The rheology of metal injection molding.* Journal of Materials Processing Technology, 2003. **137**(1-3): p. 132-137.
15. Eagleson, M., H.-D. Jakubke, and H. Jeschkeit, *Concise encyclopedia chemistry*. 1994, Berlin: W. de Gruyter.
16. Bhattarai, S.R., et al., *Novel production method and in-vitro cell compatibility of porous Ti-6Al-4V alloy disk for hard tissue engineering.* Journal of Biomedical Materials Research Part A, 2008. **86A**(2): p. 289-299.
17. Jha, N., et al., *Highly porous open cell Ti-foam using NaCl as temporary space holder through powder metallurgy route.* Materials & Design, 2013. **47**: p. 810-819.
18. Shangguan, J. and L. Guoqin, *Morphology and Thermal Behaviour of Poly(Methyl Methacrylate)/Poly(Ethylene Glycol) Semi-Interpenetrating Polymer Networks.* Journal of the Chilean Chemical Society, 2011. **56**(4): p. 918-921.
19. Hayat, M.D., et al., *Effect of PEG molecular weight on rheological properties of Ti-MIM feedstocks and water debinding behaviour.* Powder Technology, 2015. **270**: p. 296-301.

20. German, R.M. and A. Bose, *Injection molding of metals and ceramics*. 1997, Princeton, N.J.: Metal Powder Industries Federation.
21. Ahn, S., et al., *Effect of powders and binders on material properties and molding parameters in iron and stainless steel powder injection molding process.* Powder Technology, 2009. **193**(2): p. 162-169.
22. Arifvianto, B., M.A. Leeflang, and J. Zhou, *A new technique for the characterization of the water leaching behavior of space holding particles in the preparation of biomedical titanium scaffolds.* Materials Letters, 2014. **120**: p. 204-207.
23. Chen, G., et al., *Debinding behaviour of a water soluble PEG/PMMA binder for Ti metal injection moulding.* Materials Chemistry and Physics, 2013. **139**(2-3): p. 557-565.
24. Omar, M.A., et al., *Rapid debinding of 316L stainless steel injection moulded component.* Journal of Materials Processing Technology, 2003. **140**(1-3): p. 397-400.
25. Lynden-Bell, R.M.e., *Water and life : the unique properties of H2O*. 2010, Boca Raton, Fla.: CRC ; London : Taylor & Francis [distributor].
26. Carreño-Morelli, E., et al., *Porous titanium processed by powder injection moulding of titanium hydride and space holders.* Powder Metallurgy, 2014. **57**(2): p. 93-96.
27. Wen, C.E., et al., *Novel titanium foam for bone tissue engineering.* Journal of Materials Research, 2002. **17**(10): p. 2633-2639.
28. Kotan, G. and A.S. Bor, *Production and characterization of high porosity Ti-6Al-4V foam by space holder technique in powder metallurgy.* Turkish Journal of Engineering and Environmental Sciences, 2007. **31**(3): p. 149-156.
29. Hayat, M.D., et al., *Suitability of PEG/PMMA-based metal injection moulding feedstock: an experimental study.* The International Journal of Advanced Manufacturing Technology, 2015: p. 1-7.
30. Aydoğmuş, T. and Ş. Bor, *Processing of porous TiNi alloys using magnesium as space holder.* Journal of Alloys and Compounds, 2009. **478**(1-2): p. 705-710.
31. Jha, N., et al., *Titanium cenosphere syntactic foam with coarser cenosphere fabricated by powder metallurgy at lower compaction load.* Transactions of Nonferrous Metals Society of China, 2014. **24**(1): p. 89-99.
32. Sidambe, A.T., F. Derguti, and I. Todd, *Metal Injection Moulding of Low Interstitial Titanium.* Powder Metallurgy of Titanium: Powder Processing, Consolidation and Metallurgy of Titanium, 2012. **520**: p. 145-152.
33. Shibo, G., et al., *Powder injection molding of Ti–6Al–4V alloy.* Journal of Materials Processing Technology, 2006. **173**(3): p. 310-314.
34. Sidambe, A.T., et al., *Taguchi Optimization of Mim Titanium Sintering.* International Journal of Powder Metallurgy, 2011. **47**(6): p. 21-28.